Biochemistry

pubs.acs.org/biochemistry Article

Crystal Structure of the RNA Lariat Debranching Enzyme Dbr1 with Hydrolyzed Phosphorothioate RNA Product

Nathaniel E. Clark,*,⊥ Adam Katolik,⊥ Anastasia Welch, Christoph Schorl, Stephen P. Holloway, Jonathan P. Schuermann, P. John Hart, Alexander B. Taylor, Masad J. Damha,* and William G. Fairbrother*

Cite This: *Biochemistry* 2022, 61, 2933−2939 Read Online

ACCESS | Metrics & More | Article Recommendations | Supporting Information

ABSTRACT: The RNA lariat debranching enzyme is the sole enzyme responsible for hydrolyzing the 2′-5′ phosphodiester bond in RNA lariats produced by the spliceosome. Here, we test the ability of Dbr1 to hydrolyze branched RNAs (bRNAs) that contain a 2′-5′-phosphorothioate linkage, a modification commonly used to resist degradation. We attempted to cocrystallize a phosphorothioate-branched RNA (PS-bRNA) with wild-type *Entamoeba histolytica* Dbr1 (EhDbr1) but observed in-crystal hydrolysis of the phosphorothioate bond. The crystal structure revealed EhDbr1 in a product-bound state, with the hydrolyzed 2′-5′ fragment of the PS-bRNA mimicking the binding mode of the native bRNA substrate. These findings suggest that product inhibition may contribute to the kinetic mechanism of Dbr1. We show that Dbr1 enzymes cleave phosphorothioate linkages at rates ∼10,000-fold more slowly than native phosphate linkages. This new product-bound crystal structure offers atomic details, which can aid inhibitor design. Dbr1 inhibitors could be therapeutic or investigative compounds for human diseases such as human immunodeficiency virus (HIV), amyotrophic lateral sclerosis (ALS), cancer, and viral encephalitis.

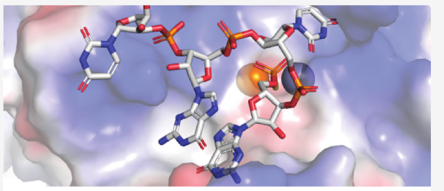

Co-crystal structure of Dbr1:RNA product

INTRODUCTION

In eucaryotic organisms, genes are composed of protein-coding exons and intervening intronic sequences. The introns are removed by the spliceosome in the production of mature messenger RNA. Due to the chemical reactions catalyzed by the spliceosome, the excised introns have a lariat configuration, where the 5′ end of the intron is covalently bonded via a 2′-5′-phosphodiester linkage to a branchpoint A residue ∼50 nts away from the 3′ end of the intron.[1,2] A single enzyme is responsible for hydrolyzing the 2′-5′-linkage, the RNA lariat debranching enzyme Dbr1.[3] Dbr1 is implicated in several biological processes, and loss of Dbr1 in humans can cause serious diseases. Class-switch recombination of immunoglobulin genes requires Dbr1, human immunodeficiency virus (HIV) replication is impaired when Dbr1 is knocked down,[4] Dbr1 loss is oncogenic,[5] and Dbr1 mutations in humans impair cell-intrinsic innate immunity in the brainstem.[6] Most cases of amyotrophic lateral sclerosis (ALS) are characterized by aggregates of the tar-DNA binding protein, TDP-43.[7,8] Ablation of the *DBR1* gene can reduce the toxicity of TDP-43 in disease models.[9] Considering these important roles in human health and diseases, an understanding of the molecular determinants of Dbr1 activity will aid efforts to design potent Dbr1 inhibitors. Such compounds could be used to study the biological role of Dbr1 and may have therapeutic benefits for diseases such as ALS or conditions where the innate immune response is problematic.

The identification of a crystallizable Dbr1 homologue from *Entamoeba histolytica* (EhDbr1) enabled structural studies of Dbr1.[10] Subsequent work demonstrated that yeast and amoeba Dbr1 require Fe^{2+}, or Fe^{2+}/Zn^{2+} for efficient debranching, and described methods for producing highly active enzymes that copurify with Fe^{2+} and Zn^{2+} cofactors.[11,12] A number of high-resolution Dbr1 structures are now available,[13] including structures of inactive Dbr1 variants in complex with branched RNA (bRNA) substrates.[12]

Phosphorothiate-modified nucleic acids are more resistant to hydrolysis than native phosphate-linked nucleic acids, and most therapeutic oligonucleotides contain phosphorothioate modifications.[14−16] Previous studies found that phosphorothioate-modified bRNAs were not hydrolyzed by Dbr1. Partially purified Dbr1 from HeLa cell extracts was unable to cleave pure R_p-2′-5′ phosphorothioate-containing RNA lariats.[17] A subsequent study demonstrated that recombinant yDbr1 had no activity against R_p-branched trinucleotides, and weak activity toward S_p-branched trinucleotides, with only a small fraction (∼<10%) of the substrate hydrolyzed in 24 h.[18] On the basis of these studies, we hypothesized that we could

Received: October 16, 2022
Revised: November 9, 2022
Published: December 9, 2022

https://doi.org/10.1021/acs.biochem.2c00590
Biochemistry 2022, 61, 2933−2939

obtain a structure of catalytically active EhDbr1 in complex with a 2′-5′ phosphorothioate-linked bRNA (PS-bRNA). Surprisingly, PS-bRNA was hydrolyzed in-crystal, and the hydrolyzed 5′ product was clearly visible in electron density maps (Figures 1−3), providing the first structure of Dbr1 in

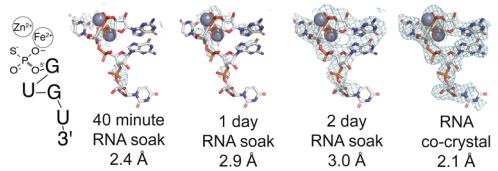

Figure 1. In-crystal cleavage of PS-bRNA. PS-bRNA was soaked in EhDbr1 crystals for 40 min, 1 day, or 2 days. Clear density for the cleaved 5′ arm of PS-bRNA appeared after 48 h. A cocrystallization experiment produced a higher-resolution structure of the PS-bRNA product (PDB 8DZK). The resolved cleavage product 5′PS-GUGU-3′ is illustrated on the left. Electron density maps contoured at 1σ. The active site metal ions are gray spheres.

complex with a product of hydrolysis. We measured the rate of phosphorothioate hydrolysis by EhDBr1 and human Dbr1 (hDbr1, Figure 4) and found that Dbr1 enzymes hydrolyze phosphorothioates 4 orders of magnitude more slowly than phosphodiesters. The new crystal structure provides new atomic details, which will inform the design of structure-based Dbr1 inhibitors.

MATERIALS AND METHODS

Synthesis of PS-bRNA and bRNA Molecules. The sequences used for crystallization (Figure 1) were based on the metazoan consensus 5′ splice site and branchpoint sequences.[19] Solid-phase synthesis of PS-bRNAs and bRNA were described previously.[20] The sequences of the bRNAs used in crystallization are shown in Figure 2C,D, and those used in enzymatic assays are shown in Figure 4C. The PS-bRNA used for cocrystallization is based on the metazoan consensus sequence (with a G instead of an A at the 3rd position from the 5′ termini, Figure 2B). Both the PS-bRNA and bRNA molecules used in the cleavage assays are based on the yeast consensus sequence (with an A at the 3rd position from the 5′ termini, Figure 4C[21]).

Protein Expression and Purification. The EhDbr1 expression plasmid (UniProt C4M1P9) was synthesized as a codon-optimized gene (GenScript) and subcloned into a modified pET 32 vector. The open reading frame consisted of an 8× HIS tag, followed by a tobacco etch virus protease site, and the EhDbr1 open reading frame. The plasmid was transformed into Bl21 *Escherichia coli* cells. Cells were cultured at 30 °C in 12× 1 L flasks using autoinduction media.[22] Cells were lysed in Ni-A buffer (50 mM Tris−HCL pH 8, 500 mM NaCl, 20 mM imidazole, 1 mM TCEP) by sonication, clarified by centrifugation, applied to a 25 mL Ni-Sepharose FF column (GE Healthcare), and eluted with a shallow gradient of Ni-B buffer (=Ni-A buffer + 400 mM imidazole). Pure fractions were pooled in a dialysis bag, mixed with a 1:50 volume of 1 mg mL^{-1} TEV protease, and dialyzed against 50 mM NaCl, 20 mM 4-(2-hydroxyethyl)-1-piperazineethanesulfonic acid (HEPES) pH 7, 1 mM ethylenediamine tetraacetic acid (EDTA), and 1 mM TCEP. After dialysis, the protein was diluted 1:5 in 10 mM sodium phosphate pH 7, applied to a 5 mL Heparin HiTrap column (GE Healthcare), and eluted with a gradient of 2 M NaCl. Pure fractions were diluted 10-fold

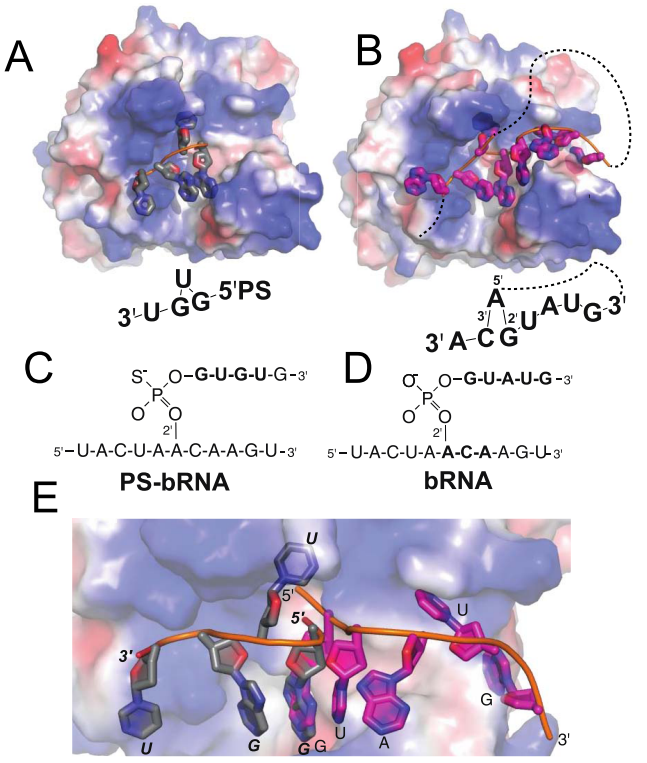

Figure 2. Comparison of the cleaved PS-bRNA cocrystal structure ((A), gray, PDB 8DZK, wt-Dbr1), with the intact bRNA cocrystal structure ((B), pink, PDB 5K78, catalytically inactive H91A−Dbr1). (A, B) Surface view of the entire RNA and binding surface. The surface is colored by the electrostatic potential to illustrate positively charged regions (blue) that interact with the phosphate backbone of RNA. RNAs are shown as cartoons. (C, D) Schematic view of the synthetic RNAs used in crystallization experiments. The nucleotides that are resolved in the crystal structures (bold) are drawn beneath the surface representation in the approximate orientations. The lariat connectivity is illustrated with a dashed line. (E). Overlay of the 5′ fragments illustrates the different binding modes, colored as in panels (A) and (B).

into 20 mM HEPES pH 7, 1 mM TCEP, and concentrated to 18 mg mL^{-1} for crystallization.

For hDbr1 (UniProt Q9UK59), the expression plasmid was synthesized as a codon-optimized gene (DNA2.0) and contained a noncleavable C-terminal 8× HIS tag. Lysis and purification were as described above, except for a Q-column that was used instead of a Heparin column (buffer A = 50 mM Tris pH 8, 50 mM NaCl, 1 mM TCEP; buffer B = A + 1 M NaCl), and there was no TEV-protease step.

Protein Crystallization. EhDbr1 (2 μL of 18 mg mL^{-1}) and crystallization solution (2 μL of 15% PEG3350, 0.4 M $LiSO_4$, 0.1 M bis-tris pH 5.5) were combined in a hanging drop plate (Nextal) over 0.25 mL of reservoir solution. After 24 h, the drops were streak-seeded from crystals that appeared in drops containing higher concentrations of PEG3350 using a cat-whisker; 3−4 days after seeding, single crystals appeared that were suitable for X-ray diffraction studies. Crystals were moved to a soak solution containing 20% PEG3350, 0.4 M $LiSO_4$, 0.1 M bis-tris pH 5.5, 7.5% glycerol, 1 mM $ZnSO_4$, and 3 mM PS-bRNA (see Figure 2C for sequence). Crystals were removed and frozen with LN2 after 40 min, 24 h, and 48 h. For the cocrystallization experiment, 1 μL of protein, 1 μL of reservoir solution, and 1 μL of soak solution were mixed and

https://doi.org/10.1021/acs.biochem.2c00590
Biochemistry 2022, 61, 2933−2939

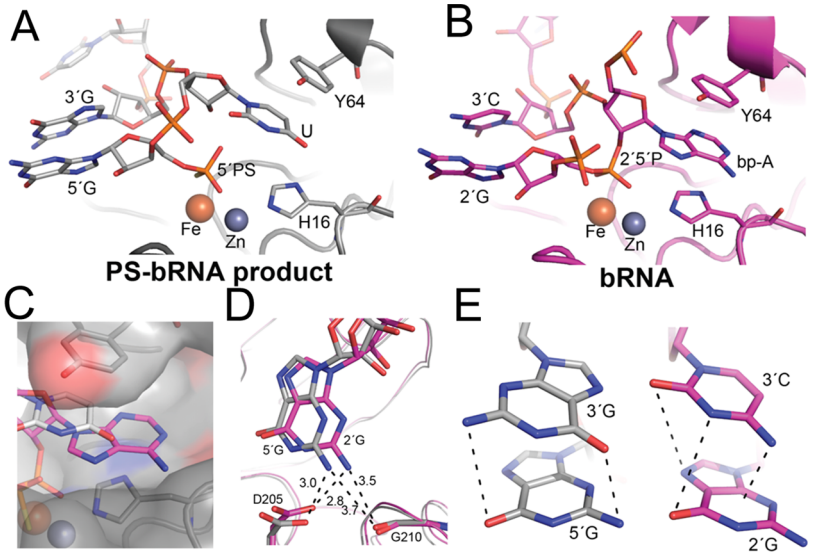

Figure 3. Active site interactions between the PS-bRNA product ((A), gray, PDB 8DZK) and bRNA ((B), pink, PDB 5K78). (A, B) EhDbr1 is shown as a ribbon, and the branchpoint-binding pockets formed by Tyr64 and His16 are shown as sticks. The Zn ion is a gray sphere, and Fe is an orange sphere. The PS-bRNA product is in panel (A), and the cocrystal structure with native bRNA is in panel (B). (C) For the PS-bRNA product, the U (gray) only partially fills the branchpoint-binding pocket (BBP) when compared to bRNA (magenta) in panel (A). (D) Hydrogen bonds between D205 and G210 and the amino group of G observed in the PS-bRNA product and bRNA structures. (E) G−G stack observed in the 5′-PS-GUGUG crystal structure (left) compared to the G−C stack in the bRNA crystal structure (right). In both structures, the stacking interactions are such that partial dipoles of opposing charges are positioned opposite each other.

equilibrated in a hanging drop plate and streak-seeded 24 h later.

X-ray Data Collection, Processing, and Model Building. Initial diffraction data were collected in-house with a Rigaku 007 source. The best crystals were sent to the Advanced Light Source (40-min, 1-day, 2-day soaks) or NE-CAT beamline 24-ID-E at Advanced Photon Source (cocrystal). Diffraction data were processed with energy-dispersive X-ray spectrum (XDS).[23] As the crystals were isomorphous with previous EhDbr1 crystals, initial maps were generated by rigid-body fitting with PDB 5K73[12] using PHENIX.[24] Based on initial maps, models were rebuilt manually in Coot,[25] and RNA was built using the R-crane plugin.[26] The data from the cocrystal structure and final model are deposited with the RCSB, PDB ID 8DZK. The RNA molecule is modeled in all five chains in the asymmetric unit, but the density is the strongest in chains A, B, and D. As the 40-min, 1-day, and 2-day soaks were of lower resolution and provided no additional structural insights relative to the high-resolution cocrystal structure, we submitted only the cocrystal structure and data to PDB. All data are available upon request. Figures were generated with PyMol (Schrodinger, LLC). Statistics for data collection and refinement are in Table S1.

Branched RNA Cleavage Assay. To measure the kinetics of Dbr1 cleavage, we used 16-mer PS-bRNA and native bRNA molecules. The sequences for these RNA molecules are presented in Figure 4C. The PS-bRNA used here differed from the one used in crystallization by a single G → A substitution in the 2′ arm. EhDbr1 (1 μM) or hDbr1 (5 μM) was combined with either bRNA (5 μM) or PS-bRNA (5 μM) in assay buffer (50 mM HEPES pH 7, 100 mM NaCl, 1 mM TCEP) at room temperature. At the indicated time points, a 3 μL aliquot was removed, added to 12 μL of water, and frozen at −80 °C. Time points were heated at 90 °C for 2 min to inactivate Dbr1; 1 μL of the diluted reactions was analyzed with a Bioanalyzer using a small RNA kit (Agilent 5067−1548). The Bioanalyzer uses microfluidic chips to perform electrophoresis in the presence of fluorescent dyes to detect separated RNAs from 6 to 150 nts. The concentration of uncleaved bRNA was quantified with instrument software (Agilent 2100 Expert), and the observed rates were estimated from plotting the resulting data in Prism and fitting with a linear regression (GraphPad). The disappearance of full-length bRNA was plotted as a function of time to estimate the rates of hydrolysis. Uncropped pseudo-electrophoretograms are presented in Figure S1. Although we were unable to test other microcapillary electrophoresis instruments (such as the Agilent TapeStation or PerkinElmer GX Touch), we suspect that these instruments would be equally suitable.

RESULTS AND DISCUSSION

Crystal Structure of EhDbr1 and PS-bRNA-1. Our initial hypothesis was that the presence of a phosphorothioate linkage would prevent hydrolysis of the PS-bRNA by EhDbr1 during structure determination. This PS-bRNA inhibits Dbr1 with an IC_{50} of 220 nM,[20] and we predicted that it would form a Dbr1:PS-bRNA complex suitable for X-ray diffraction studies. All previous structures of Dbr1:bRNA to date used catalytically inactive EhDbr1,[12] and we hypothesized that the PS-bRNA would remain intact when soaked into crystals of active Fe^{2+}/Zn^{2+}, offering a view of active-Dbr1 in complex with a bRNA. Pregrown EhDbr1 crystals were transferred to a solution of PS-bRNA and harvested after 40 min, 24 h, or 48 h of soaking. Complete diffraction data were collected for each time point. Electron density maps displayed strong density active site density at the 48 h time point (Figure 1); however, this density did not support a branched RNA model. We modeled the 2′-5′ hydrolysis product of the PS-bRNA and found good agreement with the unmodeled density. A higher-resolution cocrystal structure provided a clearer view of this fragment in complex with EhDbr1, confirming that the PS-bRNA was hydrolyzed in crystal. Four of the five nucleotides

https://doi.org/10.1021/acs.biochem.2c00590
Biochemistry 2022, 61, 2933−2939

from the 5′-PS-GUGUG-3′ fragment were clearly resolved in 3 of the 5 EhDbr1 monomers present in the asymmetric unit (Figure 1). This structure is the first example of Dbr1 bound to a cleaved RNA fragment.

The binding mode of the product mimics key features of the bRNA:EhDbr1 crystal structures. A comparison of Dbr1 with the PS-bRNA product (PDB 8DZK, Figure 2A,C) with the native bRNA substrate (PDB 5K78,[12]Figure 2B,D) illustrates how positively charged residues interact with the phosphate backbone (Figure 2A,B). The PS-bRNA product and bRNA substrate interact with the same RNA binding surfaces, but with different, incompatible binding modes (Figure 2E). In the bRNA substrate, 5K78, the 3′ terminus moves away from the catalytic center (toward the right side of the image), and in 8DZK the 3′ terminus is on the opposite side of the enzyme (toward the left side of the image), blocking the catalytic center. For the PS-bRNA product, the U nucleotide (second from the 5′ end of the cleaved product), is flipped into the branchpoint-binding pocket (BBP, discussed below), and the adjacent G residues form a G−G stack (Figure 2A). In bRNA, the branchpoint-forming A is in the BBP and adjacent C−G residues stack (Figure 2B). The PS-bRNA 5′ product occupies the region on the active site where catalysis would occur, and we hypothesize that this may represent an inhibited state. This binding mode would not be possible for the uncleaved PS-bRNA, as the 5′-UACUAACAAGU-3′ fragment would be attached to the 5′ termini (Figure 2E), resulting in a steric clash with the enzyme.

The active site of EhDbr1 features two metal ions, Zn^{2+} and Fe^{2+}, which bind the scissile 2′-5′-phosphodiester linkage. The 5′ phosphorothioate group binds to both metals in the same position occupied by the 2′-5′-phosphate in bRNA (Figure 3A,B). The branchpoint-binding pocket (BBP) is formed by His16 (a Zn ligand) at the bottom, and a conserved Tyr(64) on the top (Figure 3A,B). In a native bRNA:EhDBr1(H91A) structure (PDB 5K78),[12] the branchpoint A flips ∼180° (relative to the other nucleobases in the bRNA) into the BBP (Figure 3B). The adjacent 2′G and 3′C residues in the bRNA form an aromatic base-stacking interaction. The PS-bRNA product, 5′-PS-GUGUG-3′, places a U into the BBP, and the adjacent 5′ and 3′G residues form the stacking interaction (Figures 2A and 3A). However, the U does not fully occupy the branchpoint-binding pocket (Figure 3C), as the PS-bRNA has only 3′-5′-phosphodiester linkages, which cannot occupy the same positions as the native bRNA substrate (compare phosphate positions in Figure 3A,C).

Intron sequences begin with a 5′ GUA in yeast and a GU(G/A) in metazoa.[21] The PS-bRNA used in crystallization is based on the metazoa sequence (Figure 2C), while the bRNA used in 5K78 is based on the yeast sequence. The only sequence-specific hydrogen bonds observed in Dbr1 crystal structures are between the 5′G and the branchpoint A to which it is covalently linked through a 5′2′ phosphodiester bond. Presumably, this lack of extensive hydrogen bonding allows Dbr1 enzymes to recognize lariat substrates with diverse sequences that share a common topology conferred by the branchpoint. Interestingly, the 5′-Gs in both structures (PS-bRNA product PDB 8DZK, and bRNA substrate PDB 5K78), occupy the same space and form the same guanine-NH_2 Asp205 and Gly210 hydrogen bonds (Figure 3D).

The stacking interactions in both the PS-bRNA product and bRNA appear to be favorable as they position partial positive and negative dipoles opposite each other. In the PS-bRNA product G−G stack (Figure 3E, left), the carbonyl and amino groups of the nucleobases are opposite to each other, which may allow the partial dipoles on these groups to cancel out. For the bRNA G−C stack (Figure 3E, right), the amino group of the C is positioned at the center of the 6-member aromatic ring, and carbonyl groups are opposite the cyclic amine groups.

In summary, the product mimics four key features of native bRNA binding: (i) placing a flipped nucleotide in the branchpoint-binding pocket; (ii) favorable intramolecular stacking of nucleobases adjacent to the flipped nucleotide; (iii) ionic interactions between the positively charged protein surface and negatively charged phosphate backbone, and (iv) hydrogen bonds between the 5′G (of PS-bRNA-1) or 2′-5′G (of bRNA) and residues D205 and G210 (Figures 2 and 3).

Enzymatic Hydrolysis of PS-bRNA and bRNA in Solution. The crystal-soaking time course demonstrated that Dbr1 can hydrolyze PS-bRNA, but we could not estimate the rate of cleavage from these experiments. Although we knew the PS-bRNA concentration (3 mM), it is difficult to estimate the enzyme concentration when crystals are transferred into a drop of the substrate and to estimate the specific activity of the crystalline enzyme. Additionally, the crystallization conditions are nonphysiological, with a pH of 5.5 and high concentrations of Li_2SO_4 and poly(ethylene glycol). Therefore, we used a bRNA cleavage assay to measure how quickly EhDbr1 and hDbr1 could hydrolyze PS-bRNA and bRNA under physiological conditions.

Traditionally, bRNA cleavage assays are performed with ^{32}P-labeled samples and urea-poly(acrylamide) gel electrophoresis (PAGE).[18,27,28] However, these assays are laborious and require a considerable investment of time and laboratory resources, so we developed a nonradioactive bRNA cleavage assay. We synthesized and purified the bRNA and PS-bRNA using solid-phase synthesis, as these molecules are not commercially available. Initially, we tested if we could detect these bRNAs in urea-PAGE gels using SYBR gold stain, silver staining, and UV-shadowing. However, none of these approaches could detect the bRNAs at reasonable concentrations (∼20 pmol $lane^{-1}$, or 10 μL of 5 μM bRNA solution). Next, we tested microcapillary electrophoresis using a Bioanalyzer instrument. The Bioanalyzer reliably detected intact 16-mer bRNAs at 5 μM, and we used the disappearance of intact bRNA to measure Dbr1 cleavage rates. The 11- and 5-mer products were not well resolved (Figure S1). We found that the bRNA was cleaved very quickly by EhDbr1, with 100% cleaved at our first time point (30 s, Figure 4A). In contrast, the PS-bRNA was cleaved very slowly, with 100% cleavage occurring between the 5- and 15-h time points. We quantified the intact substrate vs time, and based on the slope of that curve (Figure 4B), we estimate that 100% PS-bRNA cleavage occurred around 7 h for EhDbr1, and 5 h with hDbr1. From the concentration of the enzyme (1 μM EhDbr1, 5 μM hDbr1 on account of lower hDbr1 specific activity) and substrate (5 μM), we calculated turnover rates of >600 h^{-1} for bRNA by EhDbr1, 0.70 h^{-1} for EhDbr1 and PS-bRNA, and 0.22 h^{-1} for hDbr1 and PS-bRNA. The bRNA rate was likely faster than 600 h^{-1} (equivalent to 0.2 s^{-1}), as rates of 2 and 5.6 s^{-1} for EhDbr1 and yDbr1 were measured in a continuous assay with a fluorescent substrate, respectively.[11,12] The high enzyme concentrations necessary to achieve cleavage of the PS-bRNA in a reasonable timeframe limited our ability to measure rates > 0.2 s^{-1}.

https://doi.org/10.1021/acs.biochem.2c00590
Biochemistry 2022, 61, 2933−2939

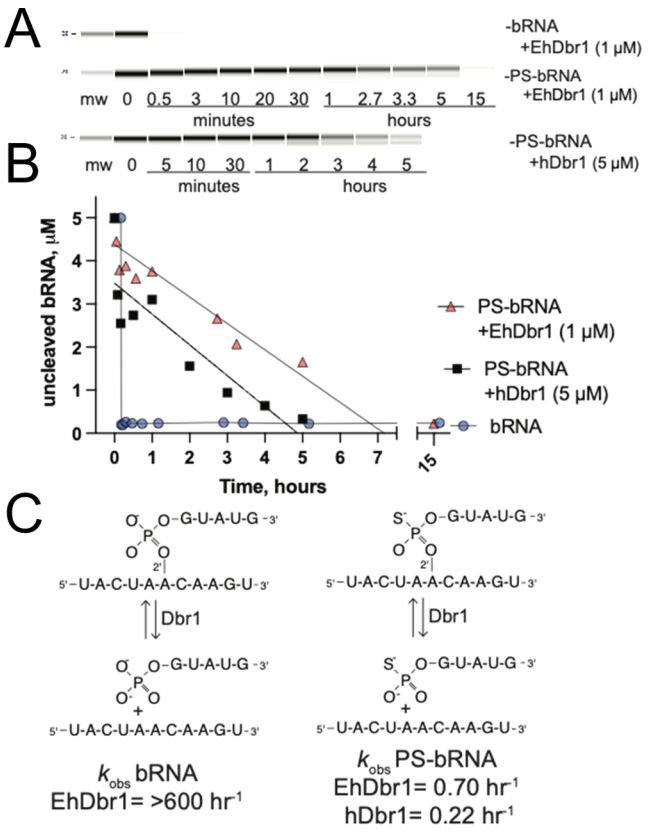

Figure 4. Kinetics of PS-bRNA and bRNA hydrolysis by EhDbr1 and hDbr1. (A) Bioanalyzer gel image showing the time course of PS-bRNA or bRNA cleavage by EhDbr1 and hDbr1. (B) Quantification of uncleaved, intact bRNA as a function of time. (C) Schematic of the hydrolysis reactions of bRNA (left) and PS-bRNA (right), with k_{obs} calculated from the plot in panel (A).

The PS-bRNA used in this assay is based on the yeast consensus sequence, while the PS-bRNA used in crystallization is based on the metazoan consensus sequence and differs by a single G → A substitution at the 3rd position of the 5′ arm (compare Figures 2–4C,[21]). We used the metazoan substrate for crystallization experiments because we had a larger quantity after synthesis and purification. The crystallization experiments consumed our entire supply of the metazoan substrate, and we switched to the yeast substrate for the hydrolysis assays. Unfortunately, we were unable to systematically test both metazoa and yeast sequences in this assay.

CONCLUSIONS

Here, we report that EhDbr1 and hDbr1 enzymes cleave phosphorothioate-linked bRNA substrates 3–4 orders of magnitude more slowly than similar phosphate-linked bRNA substrates. Dbr1 is a member of the metallophosphoesterase family of enzymes, a family of nucleases and phosphatases that use a common catalytic mechanism and share highly conserved active site residues.[29] Therefore, we hypothesize that like Dbr1, other MPEs may cleave phosphorothioate substrates.

We report a nonradioactive bRNA cleavage assay assisted by capillary electrophoresis analysis. Our results demonstrate that Dbr1 enzymes cleave both R_p and S_p phosphorothioates (Figure 4B), as our PS-bRNA was a mixture of diastereomers and was 100% cleaved. This contrasts with previous reports in which Dbr1 samples were unable to hydrolyze PS-bRNA.[17,18]

The crystal structure of EhDbr1 with the 5′-PS-GUGUG-3′ product (PDB 8DZK) is the first atomic structure of a Dbr1 enzyme in complex with a product of its hydrolysis reaction. Because the binding of the product occupies the catalytic center and is incompatible with substrate binding (Figures 2 and 3), we hypothesize that the product of Dbr1 cleavage may be inhibitory, and that product inhibition may be relevant to the kinetic mechanism of Dbr1. However further experiments would be required to test this hypothesis. The structure we report here complements previous structures of Dbr1 at different stages of catalysis[10,12] and provides atomic details for structure-based Dbr1 inhibitor design. For example, trinucleotide motifs bind the catalytic center and branchpoint-binding pockets in both the product and bRNA crystal structures (PDB 8DZK, 5K78), and small molecules that mimic these structures could be potent inhibitors. Also, as we demonstrate that phosphorothioate linkages are not as resistant to Dbr1 hydrolysis as previously believed, phosphoramidate[30] or phosphonate linkages may be preferable for Dbr1 inhibitors. We hope that these results aid the development of Dbr1 inhibitors that may illuminate the biological roles of Dbr1 in normal physiology and diseases such as viral encephalitis, cancer, and ALS.[5,6,9,31,32]

ASSOCIATED CONTENT

Supporting Information

The Supporting Information is available free of charge at https://pubs.acs.org/doi/10.1021/acs.biochem.2c00590.

Table of X-ray data and refinement statistics, and uncropped gel images of the branched RNA cleavage assay (PDF)

Accession Codes

human Dbr1: Q9UK5. *Entamoeba histolytica* Dbr1: C4M1P

AUTHOR INFORMATION

Corresponding Authors

Nathaniel E. Clark − *Department of Molecular Biology, Cell Biology, and Biochemistry, Brown University, Providence, Rhode Island 02891, United States;* orcid.org/0000-0002-5478-1610; Email: Nathaniel.clark@brown.edu

Masad J. Damha − *Department of Chemistry, McGill University, Montreal, Quebec H3A 0B8, Canada;* orcid.org/0000-0002-4458-1623; Email: masad.damha@mcgill.edu

William G. Fairbrother − *Department of Molecular Biology, Cell Biology, and Biochemistry, Brown University, Providence, Rhode Island 02891, United States;* Email: William.fairbrother@brown.edu

Authors

Adam Katolik − *Department of Chemistry, McGill University, Montreal, Quebec H3A 0B8, Canada*

Anastasia Welch − *Department of Molecular Biology, Cell Biology, and Biochemistry, Brown University, Providence, Rhode Island 02891, United States*

Christoph Schorl − *Department of Molecular Biology, Cell Biology, and Biochemistry, Brown University, Providence, Rhode Island 02891, United States*

Stephen P. Holloway − *Department of Biochemistry and Structural Biology, University of Texas Health Science Center, San Antonio, Texas 78229, United States*

Jonathan P. Schuermann − *Northeastern Collaborative Access Team, Department of Chemistry and Chemical Biology, Cornell University, Ithaca, New York 14853, United States*

P. John Hart − *Department of Biochemistry and Structural Biology, University of Texas Health Science Center, San Antonio, Texas 78229, United States*

Alexander B. Taylor − *Department of Biochemistry and Structural Biology, University of Texas Health Science Center, San Antonio, Texas 78229, United States;* orcid.org/0000-0003-3517-6033

Complete contact information is available at: https://pubs.acs.org/10.1021/acs.biochem.2c00590

Author Contributions

[⊥]N.E.C. and A.K. contributed equally.

Funding

M.J.D. was supported by a Discovery Grant from the National Science and Engineering Council of Canada (NSERC). W.G.F was supported by NIH grants R01GM105681 and R01GM127472.

Notes

The authors declare no competing financial interest.

■ ACKNOWLEDGMENTS

This work is based upon research conducted in the Structural Biology Core Facility, a part of the Institutional Research Cores at the University of Texas Health Science Center at San Antonio supported by the Office of the Vice President for Research, Greehey Children's Cancer Research Institute, the Mays Cancer Center Drug Discovery, and the Structural Biology Shared Resource (NIH P30 CA054174). This work is based upon research conducted at the Northeastern Collaborative Access Team beamlines, which are funded by the National Institute of General Medical Sciences from the National Institutes of Health (P30 GM124165). The Eiger 16 M detector on 24-ID-E is funded by an NIH-ORIP HEI grant (S10OD021527). This research used resources from the Advanced Photon Source; a U.S. Department of Energy (DOE) Office of Science User Facility operated for the DOE Office of Science by Argonne National Laboratory under contract no. DE-AC02-06CH11357.

■ REFERENCES

(1) Ruskin, B.; Krainer, A. R.; Maniatis, T.; Green, M. R. Excision of an intact intron as a novel lariat structure during pre-mRNA splicing in vitro. *Cell* **1984**, *38*, 317−331.

(2) Padgett, R. A.; Konarska, M. M.; Grabowski, P. J.; Hardy, S. F.; Sharp, P. A. Lariat RNA's as intermediates and products in the splicing of messenger RNA precursors. *Science* **1984**, *225*, 898−903.

(3) Garrey, S. M.; Katolik, A.; Prekeris, M.; Li, X.; York, K.; Bernards, S.; Fields, S.; Zhao, R.; Damha, M. J.; Hesselberth, J. R. A homolog of lariat-debranching enzyme modulates turnover of branched RNA. *RNA* **2014**, *20*, 1337−1348.

(4) Zheng, S.; Vuong, B. Q.; Vaidyanathan, B.; Lin, J. Y.; Huang, F. T.; Chaudhuri, J. Non-coding RNA Generated following Lariat Debranching Mediates Targeting of AID to DNA. *Cell* **2015**, *161*, 762−773.

(5) Han, B.; Park, H. K.; Ching, T.; Panneerselvam, J.; Wang, H.; Shen, Y.; Zhang, J.; Li, L.; Che, R.; Garmire, L.; Fei, P. Human DBR1 modulates the recycling of snRNPs to affect alternative RNA splicing and contributes to the suppression of cancer development. *Oncogene* **2017**, *36*, 5382−5391.

(6) Zhang, S. Y.; Clark, N. E.; Freije, C. A.; Pauwels, E.; Taggart, A. J.; Okada, S.; Mandel, H.; Garcia, P.; Ciancanelli, M. J.; Biran, A.; Lafaille, F. G.; Tsumura, M.; Cobat, A.; Luo, J.; Volpi, S.; Zimmer, B.; Sakata, S.; Dinis, A.; Ohara, O.; Garcia Reino, E. J.; Dobbs, K.; Hasek, M.; Holloway, S. P.; McCammon, K.; Hussong, S. A.; DeRosa, N.; Van Skike, C. E.; Katolik, A.; Lorenzo, L.; Hyodo, M.; Faria, E.; Halwani, R.; Fukuhara, R.; Smith, G. A.; Galvan, V.; Damha, M. J.; Al-Muhsen, S.; Itan, Y.; Boeke, J. D.; Notarangelo, L. D.; Studer, L.; Kobayashi, M.; Diogo, L.; Fairbrother, W. G.; Abel, L.; Rosenberg, B. R.; Hart, P. J.; Etzioni, A.; Casanova, J. L. Inborn Errors of RNA Lariat Metabolism in Humans with Brainstem Viral Infection. *Cell* **2018**, *172*, 952−965.

(7) Mackenzie, I. R. A.; Bigio, E. H.; Ince, P. G.; Geser, F.; Neumann, M.; Cairns, N. J.; Kwong, L. K.; Forman, M. S.; Ravits, J.; Stewart, H.; Eisen, A.; McClusky, L.; Kretzschmar, H. A.; Monoranu, C. M.; Highley, J. R.; Kirby, J.; Siddique, T.; Shaw, P. J.; Lee, V. M.; Trojanowski, J. Q. Pathological TDP-43 distinguishes sporadic amyotrophic lateral sclerosis from amyotrophic lateral sclerosis with SOD1 mutations. *Ann. Neurol.: Off. J. Am. Neurol. Assoc. Child Neurol. Soc.* **2007**, *61*, 427−434.

(8) Neumann, M.; Sampathu, D. M.; Kwong, L. K.; Truax, A. C.; Micsenyi, M. C.; Chou, T. T.; Bruce, J.; Schuck, T.; Grossman, M.; Clark, C. M.; McCluskey, L. F.; Miller, B. L.; Masliah, E.; Mackenzie, I. R.; Feldman, H.; Feiden, W.; Kretzschmar, H. A.; Trojanowski, J. Q.; Lee, V. M. Ubiquitinated TDP-43 in frontotemporal lobar degeneration and amyotrophic lateral sclerosis. *Science* **2006**, *314*, 130−133.

(9) Armakola, M.; Higgins, M. J.; Figley, M. D.; Barmada, S. J.; Scarborough, E. A.; Diaz, Z.; Fang, X.; Shorter, J.; Krogan, N. J.; Finkbeiner, S.; Farese, R. V., Jr.; Gitler, A. D. Inhibition of RNA lariat debranching enzyme suppresses TDP-43 toxicity in ALS disease models. *Nat. Genet.* **2012**, *44*, 1302−1309.

(10) Montemayor, E. J.; Katolik, A.; Clark, N. E.; Taylor, A. B.; Schuermann, J. P.; Combs, D. J.; Johnsson, R.; Holloway, S. P.; Stevens, S. W.; Damha, M. J.; Hart, P. J. Structural basis of lariat RNA recognition by the intron debranching enzyme Dbr1. *Nucleic Acids Res.* **2014**, *42*, 10845−10855.

(11) Clark, N. E.; Katolik, A.; Taggart, A. J.; Buerer, L.; Holloway, S.; Miller, N.; Phillips, J. D.; Farrell, C. P.; Damha, M. J.; Fairbrother, W. Metal content and kinetic properties of yeast RNA lariat debranching enzyme Dbr1. *RNA* **2022**, *28*, 927−936.

(12) Clark, N. E.; Katolik, A.; Roberts, K. M.; Taylor, A. B.; Holloway, S. P.; Schuermann, J. P.; Montemayor, E. J.; Stevens, S. W.; Fitzpatrick, P. F.; Damha, M. J.; Hart, P. J. Metal dependence and branched RNA cocrystal structures of the RNA lariat debranching enzyme Dbr1. *Proc. Natl. Acad. Sci. U.S.A.* **2016**, *113*, 14727−14732.

(13) Ransey, E.; Paredes, E.; Dey, S. K.; Das, S. R.; Heroux, A.; Macbeth, M. R. Crystal structure of the Entamoeba histolytica RNA lariat debranching enzyme EhDbr1 reveals a catalytic Zn(2+)/Mn(2+) heterobinucleation. *FEBS Lett.* **2017**, *591*, 2003−2010.

(14) Eckstein, F. Phosphorothioates, essential components of therapeutic oligonucleotides. *Nucleic Acid Ther.* **2014**, *24*, 374−387.

(15) Volk, D. E.; Lokesh, G. L. R. Development of Phosphorothioate DNA and DNA Thioaptamers. *Biomedicines* **2017**, *5*, No. 41.

(16) Corey, D. R.; Damha, M. J.; Manoharan, M. Challenges and Opportunities for Nucleic Acid Therapeutics. *Nucleic Acid Ther.* **2022**, *32*, 8−13.

(17) Maschhoff, K. L.; Padgett, R. A. The stereochemical course of the first step of pre-mRNA splicing. *Nucleic Acids Res.* **1993**, *21*, 5456−5462.

(18) Mourani, R.; Damha, M. J. Synthesis, characterization, and biological properties of small branched RNA fragments containing chiral (Rp and Sp) 2′,5′-phosphorothioate linkages. *Nucleosides, Nucleotides Nucleic Acids* **2006**, *25*, 203−229.

(19) Nam, K.; Hudson, R. H.; Chapman, K. B.; Ganeshan, K.; Damha, M. J.; Boeke, J. D. Yeast lariat debranching enzyme. Substrate and sequence specificity. *J. Biol. Chem.* **1994**, *269*, 20613−20621.

(20) Katolik, A.; Clark, N. E.; Tago, N.; Montemayor, E. J.; Hart, P. J.; Damha, M. J. Fluorescent Branched RNAs for High-Throughput Analysis of Dbr1 Enzyme Kinetics and Inhibition. *ACS Chem. Biol.* **2017**, *12*, 622−627.

(21) Li, C.; Tarn, W.-Y.Splicing. In *Encyclopedic Reference of Genomics and Proteomics in Molecular Medicine*; Springer: Berlin, Heidelberg, 2006; pp 1788−1792.
(22) Studier, F. W. Protein production by auto-induction in high density shaking cultures. *Protein Expression Purif.* **2005**, *41*, 207−234.
(23) Kabsch, W. Xds. *Acta Crystallogr., Sect. D: Biol. Crystallogr.* **2010**, *66*, 125−132.
(24) Liebschner, D.; Afonine, P. V.; Baker, M. L.; Bunkoczi, G.; Chen, V. B.; Croll, T. I.; Hintze, B.; Hung, L. W.; Jain, S.; McCoy, A. J.; Moriarty, N. W.; Oeffner, R. D.; Poon, B. K.; Prisant, M. G.; Read, R. J.; Richardson, J. S.; Richardson, D. C.; Sammito, M. D.; Sobolev, O. V.; Stockwell, D. H.; Terwilliger, T. C.; Urzhumtsev, A. G.; Videau, L. L.; Williams, C. J.; Adams, P. D. Macromolecular structure determination using X-rays, neutrons and electrons: recent developments in Phenix. *Acta Crystallogr., Sect. D: Struct. Biol.* **2019**, *75*, 861−877.
(25) Emsley, P.; Lohkamp, B.; Scott, W. G.; Cowtan, K. Features and development of Coot. *Acta Crystallogr., Sect. D: Biol. Crystallogr.* **2010**, *66*, 486−501.
(26) Keating, K. S.; Pyle, A. M. Semiautomated model building for RNA crystallography using a directed rotameric approach. *Proc. Natl. Acad. Sci. U.S.A.* **2010**, *107*, 8177−8182.
(27) Khalid, M. F.; Damha, M. J.; Shuman, S.; Schwer, B. Structure-function analysis of yeast RNA debranching enzyme (Dbr1), a manganese-dependent phosphodiesterase. *Nucleic Acids Res.* **2005**, *33*, 6349−6360.
(28) Nam, K.; Hudson, R. H.; Chapman, K. B.; Ganeshan, K.; Damha, M. J.; Boeke, J. D. Yeast lariat debranching enzyme. Substrate and sequence specificity. *J. Biol. Chem.* **1994**, *269*, 20613−20621.
(29) Matange, N.; Podobnik, M.; Visweswariah, S. S. Metallophosphoesterases: structural fidelity with functional promiscuity. *Biochem. J.* **2015**, *467*, 201−216.
(30) Tago, N.; Katolik, A.; Clark, N. E.; Montemayor, E. J.; Seio, K.; Sekine, M.; Hart, P. J.; Damha, M. J. Design, Synthesis, and Properties of Phosphoramidate 2′,5′-Linked Branched RNA: Toward the Rational Design of Inhibitors of the RNA Lariat Debranching Enzyme. *J. Org. Chem.* **2015**, *80*, 10108−10118.
(31) Galvis, A. E.; Fisher, H. E.; Fan, H.; Camerini, D. Conformational Changes in the 5′ End of the HIV-1 Genome Dependent on the Debranching Enzyme DBR1 during Early Stages of Infection. *J. Virol.* **2017**, *91*, No. e01377-17.
(32) Ye, Y.; De Leon, J.; Yokoyama, N.; Naidu, Y.; Camerini, D. DBR1 siRNA inhibition of HIV-1 replication. *Retrovirology* **2005**, *2*, No. 63.

https://doi.org/10.1021/acs.biochem.2c00590
Biochemistry 2022, 61, 2933−2939